12

DENDRITIC SPINES

Dendritic spines, sometimes also called dendritic thorns, are tiny, specialized protoplasmic protuberances that cover the surface of many neurons. First described by Ramón y Cajal (1909; 1991) in light-microscopic studies of Golgi stained tissue, they are among the most striking subneuronal features of many neurons. Indeed, the presence of a high density of dendritic spines allows the unambiguous classification of neuronal types into *spiny* and *aspiny*, *sparsely spiny*, or *smooth* neurons. Over 90% of all excitatory synapses that occur in the cortex are located on dendritic spines. Spines can be found in all vertebrates as well as in invertebrates (e.g., the dendrites of Kenyon cells in the mushroom bodies in the olfactory system of the insect brain). The intimate association of spines with synaptic traffic suggests some crucial role in synaptic transmission and plasticity.

Because of their submicrometer size (see below), physiological hypotheses as to the function of dendritic spines have only very recently become accessible to the experimentalist. For the previous two decades, spine properties have been investigated through analytical and computational studies based on morphological data, providing a very fertile ground for the crosspollination of theory and experiment. (For a very readable historical account of this see Segev et al., 1995.) The recent technical advances in the direct visualization of calcium dynamics in dendrites and spines are now permitting direct tests of some of these theoretical inferences (Guthrie, Segal, and Kater, 1991; Müller and Connor, 1991; Yuste and Denk, 1995; Denk, Sugimori, and Llinás, 1995; Svoboda, Tank, and Denk, 1996). As discussed in this chapter and, more extensively, in Chap. 19, the theoretical models that have endowed spines with active properties giving rise to all-or-none behavior (Perkel and Perkel, 1985; Shepherd et al., 1985; Segev and Rall, 1988; Baer and Rinzel, 1991) have, in general, been confirmed experimentally.

Historically, the possibility of implementing synaptic memory by modulating the electroanatomy of spines was recognized early on (Chang, 1952) and was subsequently analyzed in depth by Rall (1970, 1974, 1978) and many others. Because small changes in the spine morphology can lead to large changes in the amplitude of the EPSP induced by the excitatory synapse on the spine, spines have been considered to contribute to the modulation of synaptic "weight" during long-term potentiation (see Chap. 13). In a radical extension of this original idea, Crick (1982) advanced the "twitching spine" hypothesis, the notion that spines, using actin-based contractile machinery in the spine neck, could subserve very fast changes (less

than a second) in synaptic efficacy, and that this might provide a mechanism for short-term memory. Remarkably, it has now been shown in cultured hippocampal neurons that spines can change their shape within seconds (Fischer et al., 1998).

Within the last years the focus of research has shifted away from the electrical properties of spines toward their ability to provide a local and isolated biochemical compartment for calcium and other second messengers underlying the induction and expression of synaptic plasticity (for the first clear statement of this, see Shepherd, 1972, 1978; for reviews, see Koch and Zador, 1993; Harris and Kater, 1994; Shepherd, 1996). Furthermore, spines have also been treated as devices subserving highly localized "pseudological" computations.

We begin this chapter by reviewing the natural history of spines before we analyze their electrical properties and show how dendrites studded with spines can be reduced to smooth dendrites in terms of the solution of the associated linear cable equation. We defer a thorough discussion of the threshold type of logical computations that can be carried out in spines with HH-like membranes to Sec. 19.3.2. Finally, we apply the concepts introduced in the previous chapter to understand why spines can serve as a microenvironment for highly local calcium changes that serve to isolate synapses on the spine from the dendrite and vice versa.

12.1 Natural History of Spines

In the following, we review some of the pertinent facts concerning the structure, size, and distribution of dendritic spines.

12.1.1 Distribution of Spines

Neurons in different parts of the brain can be classified into two groups according to whether or not their dendrites are studded with spines. *Spiny* neurons include pyramidal and stellate cells and account for about three-quarters of the neurons in the neocortex, while *smooth* cells, whose dendrites carry few or no spines, make up the remainder. Smooth cells include basket cells, chandelier or axo-axonic cells, and double-bouquet cells, and stain for the inhibitory neurotransmitter GABA (Douglas and Martin, 1998). It is at present a mystery why one class of cortical cells, inhibitory interneurons, should have no spines, while excitatory cells have so many.

It is important to realize that in many parts of the brain outside of the cortex, inhibitory cells can be covered with spines. Two of the best known examples are the Purkinje cells in the cerebellum (Llinás and Walton, 1998) and the principal cells in the neostriatum (Kawaguchi, Wilson, and Emson, 1990; Wilson, 1998). Both are covered by spines, both use an inhibitory neurotransmitter, and both constitute the only output of their respective systems (Fig. 12.1).

Indeed, the proper generalization appears to be that spiny cells are the principal output cell class of their particular brain area (frequently also referred to as *projection cells*; Shepherd, 1998).

Spines are numerous. A large layer 5 pyramidal cell in the visual cortex may have as many as 15,000 spines, averaging about two spines per micrometer of dendrite (Larkman, 1991), while the density for CA1 pyramidal cells varies from about one to five spines per micrometer of dendrite, depending on the staining method used (Harris and Stevens, 1989; Amaral, Ishizuka, and Claiborne, 1990). The inhibitory projection cells in the neostriatum have a peak density of four to six spines per micrometer of dendrite (Wilson et al., 1983). The record, though, is held by cells in the human cerebellum, where individual Purkinje

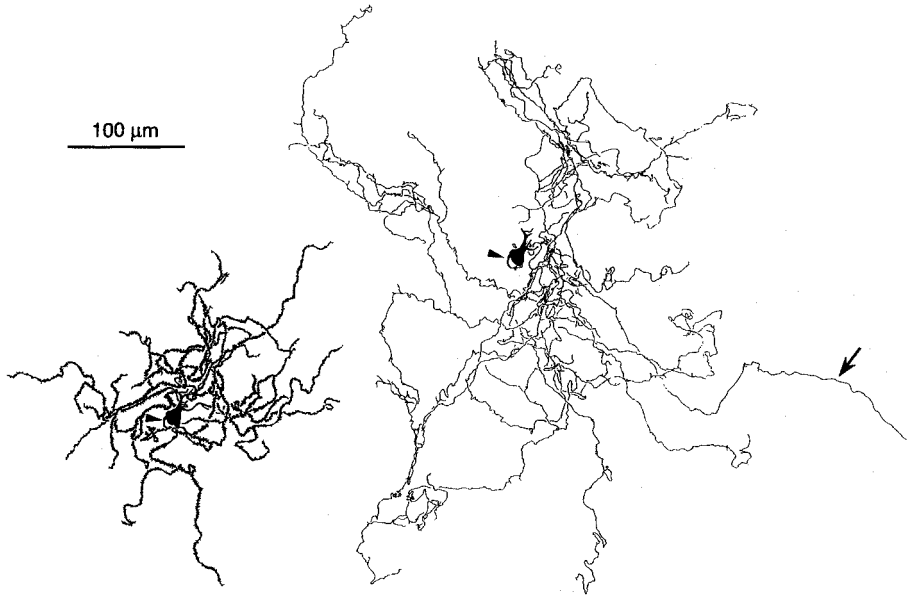

Fig. 12.1 SPINY INHIBITORY NEURON Dendritic (left) and axonal (right) arborization of a projection cell in the rat neostriatum, part of the basal ganglia, that was injected with biocytin and reconstructed. The dendrites are covered by up to five spines per micrometer. In the human, three-quarters of the approximately 110 million neostriatum neurons are of this type. They make both local connections, as illustrated here, and leave the neostriatum (elongated arrow) to terminate in the globus pallidus. These axons are the only output of the neostriatum and have an *inhibitory* effect on their postsynaptic target. Spiny cells in neocortex and hippocampus, in contrast, are excitatory. Reprinted by permission from Kawaguchi, Wilson, and Emson (1990).

cells are studded by up to 200,000 spines, each spine carrying a single excitatory synapse from a parallel fiber (Braitenberg and Atwood, 1958; Harris and Stevens, 1988b).

12.1.2 Microanatomy of Spines

Spines are found in a wide variety of shapes (Jones and Powell, 1969; Peters and Kaiserman-Abramof, 1970; Woolf, Shepherd, and Greer, 1991a,b; Figs. 12.2–12.4), ranging from short and stubby, through the archetypal "mushroom shaped," to long and thin ones. Many spines branch. In the case of spines on CA3 hippocampal pyramidal cells receiving mossy fiber inputs, up to 16 branches have been observed to emerge from a single dendritic origin (Chicurel and Harris, 1992).

Given the diversity of spine shapes (Fig. 12.4), it is not easy to define the "average" spine. However, most spines show a clearly differentiated "neck" and a "head." Their exact morphology can best be appreciated via three-dimensional reconstructions of serial electron micrographs of the entire cell (a heroic task) as carried out by White and Rock (1980) in the mouse somatosensory cortex, by Wilson et al., (1983) in the neostriatum, and by Harris and Stevens (1988a,b, 1989) in the cerebellum and the cortex. For CA1 pyramidal cells in the rat hippocampus, Harris and Stevens (1989) found wide variability in the dimensions of spines, with spine necks ranging in length from 0.08 to 1.58 μm and in diameter from 0.04 to 0.46 μm. The total volume ranges from 0.04 to 0.56 μm^3 (Fig. 12.4; see also Segev

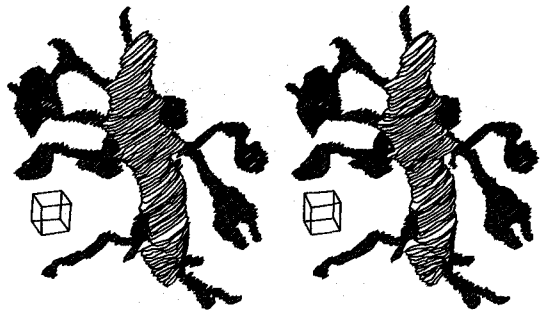

Fig. 12.2 Stereo View of a Spiny Dendrite Stereoscopic view of a portion of a spiny dendrite (of the type shown in Fig. 12.1) in the rat neostriatum. The large number of spines springing from the dendrite can be viewed in depth by focusing the eyes at a point at infinity (that is, by looking through the image). The reconstruction has been performed using high-voltage electron-microscopic axial tomography from a single 3-μm-thick section. The cube has a dimension of 0.5 μm on each side. Reprinted by permission from Wilson et al., (1992).

Fig. 12.3 Dendritic Spines in the Hippocampus Three-dimensional reconstruction of a piece of dendrite from a CA1 pyramidal cell of the rat hippocampus. There are between one and three spines per micrometer of dendrite. The diversity in the morphologies and dimensions of spines is striking. Reprinted by permission from Harris and Stevens (1989).

et al., 1995). Larger spine heads are associated with larger synapses—as measured by the size of the associated postsynaptic density—and more vesicles in the presynaptic axonal varicosity.

These dimensions indicate how spines bridge the gap between molecular and cellular scales: at a resting concentration of 80 nM and for the average spine head volume of 0.05 μm^3, only about two unbuffered Ca^{2+} ions are expected to be found in a spine head.

Dendritic spines appear to be filled with complex cellular machinery (for an overview, see Harris and Kater, 1994), most notably a specialized form of smooth endoplasmic reticulum termed the *spine apparatus*. The membranes making up the spine apparatus are closely apposed to the plasma membrane of the spine neck and appear to sequester calcium (Fifková, Markham, and Delay, 1983; Burgoyne, Gray, and Barron, 1983).

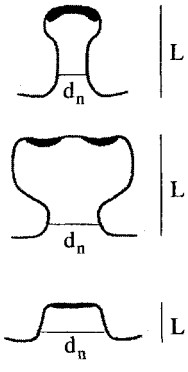

Type of Spine	d_n (μm)	L (μm)	Area (μm^2)	Volume (μm^3)
Thin	0.10 ± 0.03	0.98 ± 0.42	0.59 ± 0.29	0.04 ± 0.02
Mushroom	0.20 ± 0.07	1.50 ± 0.25	2.70 ± 0.93	0.29 ± 0.13
Stubby	0.32 ± 0.13	0.44 ± 0.15	0.45 ± 0.14	0.03 ± 0.01

Fig. 12.4 DIVERSITY OF SPINE SHAPES Three most frequent types of spine shapes in the cortex with some of their dimensions: spine neck diameter d_n, total length L, surface area, and volume. The length of the spine neck l_n is 0.51 ± 0.34 μm for thin spines and 0.43 ± 0.21 μm for mushroom-type spines. All values are averages and standard deviations. Black areas indicate the postsynaptic densities (PSD) of the asymmetric excitatory synapses on the spines. Frequently more than one synapse is located on a spine. Stubby spines are also known as "sessile." The data are measured from electron-microscopic reconstructions of spines on adult rat CA1 hippocampal pyramidal cells. Reprinted in modified form by permission from Harris, Jensen, and Tsao (1992).

Other cellular organs, such as mitochondria, microtubules, or ribosomes, are usually absent. An exception are the spines on granule cell dendrites, which make reciprocal dendrodendritic synapses with projection neurons in the mammalian olfactory bulb (Rall et al., 1966; Cameron, Kaliszewski, and Greer, 1991; Sec. 5.3). Here the mitochondria are most likely needed to provide energy to subserve presynaptic functions. Although spines lack neurofilaments, spine heads contain a dense network of actin filaments (Fischer et al., 1998). In the neck, actin filaments are oriented lengthwise along the spine apparatus (Fifková, 1985). A number of proteins known to be involved in actin-mediated activities, such as neuronal myosin (Drenckhahn and Kaiser, 1983), fodrin (Carlin, Bartelt, and Siekevitz, 1983) and calmodulin (Caceres et al., 1983), have been found in dendritic spines.

The close association of spines with the terminal boutons of axons prompted early speculation that spines might conduct impulses between neurons (Ramón y Cajal, 1909). Electron microscopic studies have since confirmed that spines are indeed the major postsynaptic target of excitatory (asymmetric, type I) synaptic input (Gray, 1959). For instance, in cat visual cortex, 93% of the afferent geniculate terminals in layer 4 is located on spines (LeVay, 1986), while a similarly high percentage is observed in the Schaffer projection from CA3 cells onto CA1 pyramidal cells in the hippocampus. Note, however, that not all excitatory pathways terminate on spines. For instance, about 70% of the excitatory synapses from layer 6 pyramidal cells terminates directly on the dendrites of layer 4 spiny stellate cells, and only a bit less than one-third of layer 6 synapses chooses spines as their termination zones (Ahmed et al., 1994). As mentioned before, excitatory projections onto inhibitory cells always make a synapse directly onto the dendrites since these cells lack spines.

Interestingly, the association between spines and synapses is limited to excitatory traffic. Inhibitory (symmetric, type II) profiles are only observed at a small fraction (between 5 and 20%) of spines in the cortex, but usually in conjunction with excitatory synapses and

never by themselves (Jones and Powell, 1969; Dehay et al., 1991; Fifková, Eason, and Schaner, 1992).

12.1.3 Induced Changes in Spine Morphology

Both the absolute number and the shape of spines can change—sometimes quite drastically—in the young and in the mature animal, and also as a function of external stimulation.

During development, absolute spine density can more than double relative to densities in the adult. Yet this increase does not occur homogeneously across all spines. Rather, thin, branched, and certain types of mushroom spines increase fourfold in density (between 2 weeks postnatal and adulthood in the rat hippocampus), while stubby spines decrease by more than half (Harris and Stevens, 1989; Harris, Jensen, and Tsao, 1992; see also Schüz, 1986; Papa et al., 1995; and Fig. 12.4). In adult female rats, the dendritic spine density on CA1 hippocampal pyramidal cells varies by 30% or more over the five-day estrus cycle, while pyramidal cells in the CA3 region show little statistically significant variation (Woolley et al., 1990). It is not known whether the number of synapses also varies by this fraction, or whether it is just the spines that wax and wane, but this certainly makes for a very dynamic environment.

Other studies have shown that the shape of spines—in particular the length and diameter of the neck—can change in response to behavioral or environmental cues such as light, social interaction, or one-shot learning or exploratory motor activity (Purpura, 1974; Coss and Globus, 1978; Bradley and Horn, 1979; Brandon and Coss, 1982; Rausch and Scheich, 1982; Lowndes and Stewart, 1994; Moser, Trommald, and Andersen, 1994).

As discussed in the following chapter, long-term potentiation (LTP), the best studied form of synaptic plasticity, is induced by brief high-frequency electrical stimulation. In the hippocampus, stimulating cells in this manner causes alterations in the spine structure (Van Harrefeld and Fifková, 1975; Lee et al., 1980; Greenough and Chang, 1985; Desmond and Levy, 1990; Calverly and Jones, 1990; Harris, Jensen and Tsao, 1992). Some of the reported changes include larger spine heads, distortions in the shape of the spine stem, an increased incidence of concave spine heads, and an increase in the number of shaft synapses. It is not known what role—if any—the changes in spine shape play in the increase in synaptic efficacy (see also Desmond and Levy, 1988). Remarkably, some of these changes in spine shape occur within seconds, mediated by actin filaments (Fischer et al., 1998).

12.2 Spines only Connect

Most of the early hypotheses considered the establishment of physical contact with presynaptic terminals as the main function of spines. (For a modern view of this, see Swindale, 1981.) It was argued that because dendritic space is scarce, spines provide additional membrane areas for synapses to make contact with. This idea has been largely dismissed, however, because electron microscopic views of spiny dendrites show that the dendritic membrane between spines often lacks synapses.

On the basis of their three-dimensional electron-microscopic reconstructions, Harris and Stevens (1988a) estimate that 29–45% of the dendritic membrane area of Purkinje cells would have been covered by synapses if all spines had been deleted and the associated synapses moved onto the dendrites. For CA1 pyramidal cell dendrites, only 5–9% of the total dendritic surface area would have been covered by the spine synapses (Harris and

Stevens, 1988a), arguing against the hypothesis that spines are necessary to supplement the dendritic membrane area available for synaptic contacts. This is corroborated by the observation (Schüz and Dortenmann, 1987) that the density of excitatory synapses on nonspiny dendrites in the cortex exceeds the spine density of pyramidal cell dendrites.

These results do not, however, address whether spines play a role in streamlining the layout of axonal and dendritic processes in the three-dimensional neuropil. It is certainly true that for a fixed dendritic radius, spiny dendrites sample a larger brain volume than dendrites devoid of spines (indeed, the latter tend to be thicker than the former; Harris and Kater, 1994).

In order to understand the functional theories that have been proposed to explain the existence of spines, we need to study their electrical properties and their ability to compartmentalize various important biological molecules.

12.3 Passive Electrical Properties of Single Spines

Rall (1974, 1978) was the first researcher to analyze the properties of passive spines, followed by many others (Wilson, 1984; Turner, 1984; Koch and Poggio, 1983a,b; Brown et al., 1988). We here follow the derivation of Koch and Poggio (1983b).

12.3.1 Current Injection into a Spine

The principal idea can be understood in terms of the simplified electrical circuit of a passive spine attached to a dendrite (Fig. 12.5). Any current injected into the spine head must flow either across the spine head resistance R_h and capacitance C_h or down through the spine neck impedance and into the dendrite. Neglecting capacitive and cable properties of the neck—due to its tiny size—we model the spine neck resistance as that of a cylinder of length l_n, diameter d_n, and resistivity R_i,

$$R_n = \frac{4R_i l_n}{\pi d_n^2}. \tag{12.1}$$

The input impedance of the spine head membrane can be described by the complex function

$$\tilde{K}_h(f) = \frac{R_h}{1 + if\tau_m} \tag{12.2}$$

where $\tau_m = R_h C_h = R_m C_m$. Because R_h is inversely proportional to the spine head area, for average spine dimensions, $R_h > 1000\,\mathrm{G}\Omega$.

The input impedance at the spine head $\tilde{K}_{sp,sp}(f)$ is determined by current flowing either through the spine head or through the spine neck. Remembering the way parallel resistances add, we have

$$\frac{1}{\tilde{K}_{sp,sp}(f)} = \frac{1}{\tilde{K}_{dd}(f) + R_n} + \frac{1}{\tilde{K}_h(f)} \tag{12.3}$$

where $\tilde{K}_{dd}(f)$ is the dendritic input impedance. Because for the entire relevant frequency range (up to hundreds of kilohertz) the spine head impedance is so much bigger than the sum of the spine neck resistance and the dendritic input impedance, we obtain the simple additive relationship between spine and dendritic input impedance,

$$\tilde{K}_{sp,sp}(f) \approx \tilde{K}_{dd}(f) + R_n. \tag{12.4}$$

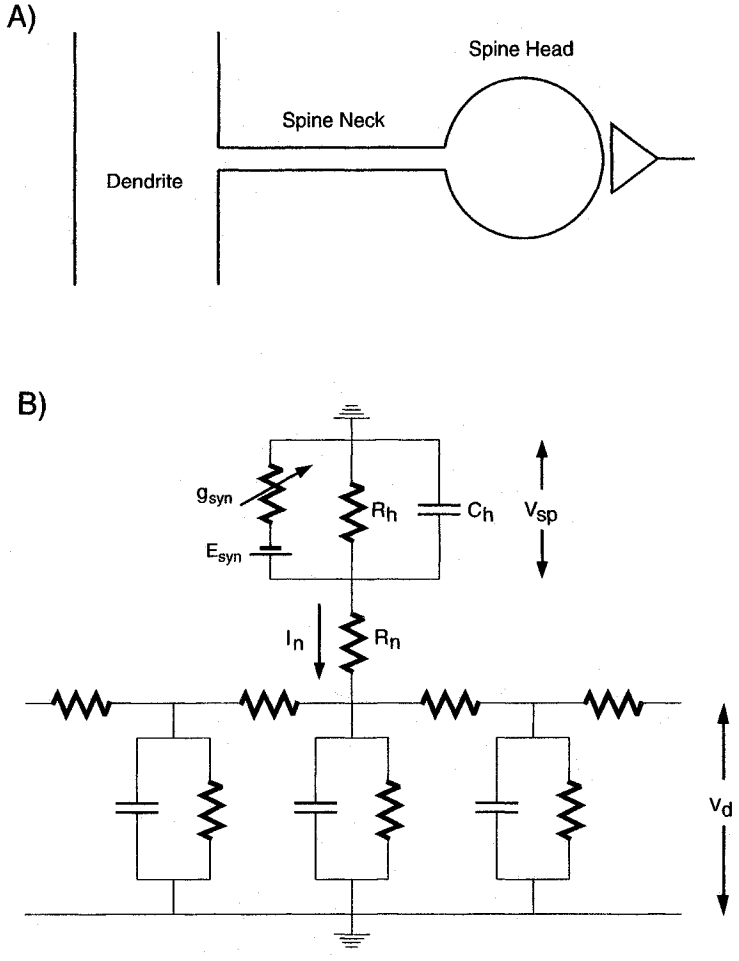

Fig. 12.5 Electrical Model of a Passive Spine **(A)** Schema of a spine with a single synaptic input on a passive dendrite. Drawn to scale, the dendrite is 0.63 μm thick, the spine head has a diameter of 0.7 μm, and the spine neck has dimensions of $d_n = 0.1$ μm and $l_n = 1$ μm. With $R_i = 200$ Ω·cm, the spine neck resistance is 254 MΩ (Eq. 12.1). With a spine neck half as thick, R_n quadruples to just beyond 1 GΩ. **(B)** Lumped electrical model of such a spine, described by an RC "head" compartment attached through an ohmic neck resistance R_n to the parent dendrite. Due to its small size, the cable and capacitive properties of the neck can be neglected.

Solving directly for the transfer impedance from the spine to the parent dendrite on the basis of Fig. 12.5 while assuming that no current loss occurs across the spine head membrane up to very high frequencies, leads to

$$\tilde{K}_{sp,d}(f) \approx \tilde{K}_{dd}(f)\,. \tag{12.5}$$

Numerically, the two last equations hold to within a small fraction of a percent (Koch and Poggio, 1983b). By exploiting transitivity (Eq. 3.29), we can write an expression for the transfer impedance from the spine to any point i in the dendritic tree as

$$\tilde{K}_{sp,i}(f) = \frac{\tilde{K}_{sp,d}(f)\tilde{K}_{di}(f)}{\tilde{K}_{dd}(f)} \approx \tilde{K}_{di}(f)\,. \tag{12.6}$$

In other words, the depolarization at any point i in a passive dendritic tree due to a spine input is identical to the EPSP caused by the same current injected into the dendrite at the base of the spine. Or, put more succinctly, electrically speaking, "spines don't matter in the linear case" (Koch and Poggio, 1985c). The reason why any current injected into the spine will reach the dendrite is that practically no current is lost across the membrane of the spine head and neck.

However, it should be noted that the membrane potential in the spine neck might need to exceed some critical threshold value to be able to initiate some biochemical event (such as those leading to long-term potentiation, as described in Chap. 13). If a synapse were made directly on the dendrite, it would require a far larger conductance change to achieve the same EPSP amplitude than a synapse on a spine. Thus, spines might matter for essentially "local" reasons (see below and Segev et al., 1995).

12.3.2 Excitatory Synaptic Input to a Spine

As discussed above, spines always appear to carry at least one excitatory synapse (Fig. 12.5). We can express the current flowing across this synapse as

$$I_{\text{syn}}(t) = g_{\text{syn}}(t)(E_{\text{syn}} - V_{sp}(t)) \tag{12.7}$$

where V_{sp} is the EPSP at the spine head. Applying Ohm's law, we arrive at

$$V_{sp}(t) = K_{sp,sp}(t) * \left(g_{\text{syn}}(t)(E_{\text{syn}} - V_{sp}(t))\right) . \tag{12.8}$$

Dealing first with stationary (or slowly varying) synaptic input, we can express the steady-state amplitude of the spine EPSP as

$$V_{sp} = \frac{g_{\text{syn}} \tilde{K}_{sp,sp} E_{\text{syn}}}{1 + g_{\text{syn}} \tilde{K}_{sp,sp}} \tag{12.9}$$

where $\tilde{K}_{sp,sp}$ corresponds to the amplitude of the steady-state spine input resistance. By the judicious use of Ohm's and Kirchhoff's laws, we can derive a similar expression for V_d, the EPSP in the dendrite just below the spine,

$$V_d = \frac{g_{\text{syn}} \tilde{K}_{dd} E_{\text{syn}}}{1 + g_{\text{syn}} \tilde{K}_{sp,sp}} = \frac{g_{\text{syn}} \tilde{K}_{dd} E_{\text{syn}}}{1 + g_{\text{syn}} (\tilde{K}_{dd} + R_n)} . \tag{12.10}$$

Let us consider these equations in the case of very small and very large synaptic input.

If the product of the synaptic conductance change g_{syn} and the spine input resistance $\tilde{K}_{sp,sp}$ is much less than 1, the numerator in Eqs. 12.9 and 12.10 can be approximated by 1 and the spine and dendritic EPSPs can be expressed as

$$V_{sp} \approx g_{\text{syn}} \tilde{K}_{sp,sp} E_{\text{syn}} \tag{12.11}$$

and

$$V_d \approx g_{\text{syn}} \tilde{K}_{dd} E_{\text{syn}} . \tag{12.12}$$

In other words, if the synaptic-induced conductance change g_{syn} is small relative to the spine input conductance $1/\tilde{K}_{sp,sp}$, the action of the synapse can be approximated by a constant current source of amplitude $g_{\text{syn}} E_{\text{syn}}$. As we saw above, spines do not matter in this limit. More specifically, changes in spine morphology have no effect on the dendritic potential just below the spine. Note, however, that this does *not* imply that the spine EPSP is identical to the dendritic EPSP; they are not. Indeed, the dendritic EPSP will be attenuated

with respect to the spine EPSP by a factor of $V_d/V_{sp} = \tilde{K}_{dd}/(\tilde{K}_{dd} + R_n)$ (Kawato and Tsukahara, 1983; Turner, 1984; Koch and Poggio, 1985c).

At the other extreme, if g_{syn} is large (that is, if $g_{\text{syn}}\tilde{K}_{sp,sp} \gg 1$), the voltage at the spine head saturates and the spine potential converges toward the synaptic reversal potential

$$V_{sp} \rightarrow E_{\text{syn}} \tag{12.13}$$

while the dendritic EPSP converges to

$$V_d \rightarrow \frac{\tilde{K}_{dd}E_{\text{syn}}}{\tilde{K}_{sp,sp}} = \frac{\tilde{K}_{dd}E_{\text{syn}}}{\tilde{K}_{dd} + R_n}. \tag{12.14}$$

Because in this regime the synapse-spine complex acts as a voltage—rather than a current—source, that is, like a battery, changes in the geometry of the spine neck will—via changes in R_n—affect the amount of synaptic current entering the spine head. Under these conditions, changes in spine morphology will change the effective "weight" of the synapse.

Figure 12.6A indicates graphically how stretching or squishing the spine neck, keeping its membrane area constant, affects the somatic EPSP for a sustained synaptic input of $g_{\text{peak}} = 1$ nS. Spine geometry only plays a role for very thin and elongated spines, when $g_{\text{peak}} > 1/R_n$ (the curve bends around $d_n = 0.05$ μm, where $g_{\text{peak}} \approx 1/R_n$). For transient inputs, very similar considerations apply (Fig. 12.6A and B). Owing to the very small membrane area of the spine head, the total spine capacity is exceedingly small, leading to very large impedance values even at high frequencies. Thus, relative independence of the dendritic membrane potential for small conductance inputs and saturation for large inputs also hold for very rapid inputs (Fig. 12.6). Spine neck geometry can affect the weight of the synapse significantly if the spine starts out very thin and elongated and becomes very short and chubby. (However, a factor of 5 change of the somatic EPSP requires an order of magnitude change in both l_n and d_n.)

Depending on the product of the synaptic conductance change and the spine input resistance, $g_{\text{syn}}\tilde{K}_{sp,sp} = g_{\text{syn}}(\tilde{K}_{dd} + R_n)$, the spine-synapse complex will thus tend to act either more as a current or as a voltage source, constraining the extent to which the morphology of the spine can alter the synaptic efficiency of the synapse. An additional requirement for the spine shape to influence the synaptic weight is that R_n needs to be large compared to the dendritic input resistance. Otherwise, modulating R_n will have little or no effect on $\tilde{K}_{sp,sp}$ (Eq. 12.10).

We can now pose the critical question: are spines elongated and thin enough to be able to effectively modulate synaptic weight? Technical advances in the last decade have provided sufficient data to estimate the spine operating regime. Probably the most complete data are available at the Schaffer collateral input to region CA1 pyramidal cells in the hippocampus. Here, the experimental estimates of g_{syn} are 0.05–0.2 nS for the fast voltage-independent AMPA synaptic component (Bekkers, Richerson, and Stevens, 1990; Malinow and Tsien, 1990) and less than 0.5 nS for the NMDA component (Bashir et al., 1991).

Based on their reconstruction of spines in the same region, Harris and Stevens (1988b, 1989) estimate the spine neck conductance $G_n = 1/R_n$ to lie mainly between 18 and 138 nS, making the critical ratio g_{syn}/G_n very small. Even taking account of the *spine apparatus*, the smooth endoplasmic reticulum that partly occludes the spine neck, does not change this conclusion appreciably. Svoboda, Tank, and Denk (1996), on the basis of high-resolution two-photon microscopy, directly estimated the diffusive and resistive coupling between the spine head and its parent dendrite, concluding with a lower bound on G_n of 7 nS.

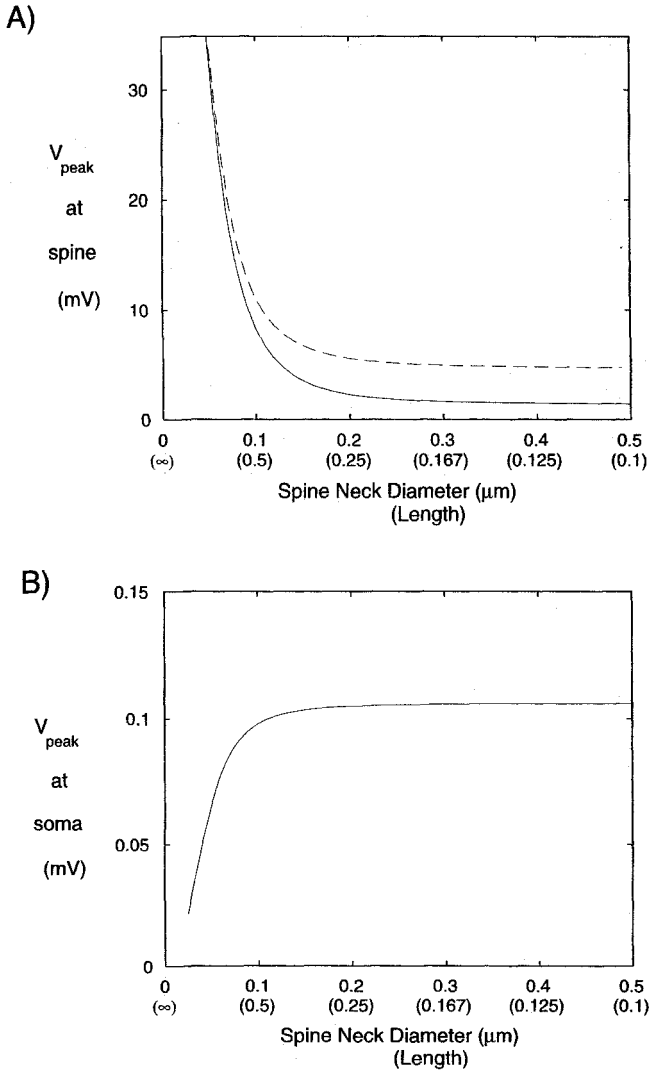

Fig. 12.6 How Do Changes in Spine Neck Geometry Affect Synaptic Weight? Neck length l_n of a single spine is varied in the presence of a single fast (t_{peak} = 0.5 msec) voltage-independent excitatory synapse (g_{peak} = 1 nS) on a spine along the upper portion of the apical tree in the layer 5 pyramidal cell (around location *a*1 in Fig. 3.7). We here assume that the total surface area of the spine neck remains constant (at 0.157 μm^2) as d_n (upper part of label on x axis) is changed, implying that the spine neck length l_n (lower part of label on x axis) changes inversely. It follows from Eq. 12.1 that the spine neck resistance scales as d_n^{-3}. The resultant EPSP is computed at the spine head itself (in **A**) as well as at the soma (in **B**). Experimental estimates of the spine neck resistance R_n are below 150 MΩ, corresponding here to values of $d_n > 0.15$ μm, falling on the portion of the curve that is relatively flat. Given the large spine neck conductance relative to the peak synaptic conductance change (estimated to be about 0.2 nS for the AMPA component), changes in spine geometry are likely to have only a minor effect on the size of the associated EPSP. In other words, postsynaptic changes in spine geometry are unlikely to implement synaptic "weight" changes. The dotted curve in **A** corresponds to the steady-state change in membrane potential in response to a sustained conductance input of the same amplitude as the transient input. When the spine is shielded from any dendritic capacitance, that is, for $d_n \rightarrow 0$, the capacitance of the spine itself can be neglected.

In agreement with earlier estimates of spine dimensions (Wilson, 1984; Turner, 1984; Brown et al., 1988), we conclude that the hippocampal projection onto spines on CA1 pyramidal cells acts as a current source and that changing the morphology of these spines most likely does not affect the associated dendritic EPSP. A similar conclusion has also been reached for a reconstructed spiny stellate cell in somatosensory cortex (Segev et al., 1995).

A different way to understand this is to ask: What effective synaptic conductance does an excitatory synapse directly on the dendrite need to possess in order to inject the same current as an excitatory synapse of amplitude g_{syn} on a spine? Neglecting all capacitive effects and any other synaptic input, the single spine will inject the current $I_n = g_{syn}E_{syn}/(1 + R_n g_{syn})$ into the dendrite. Thus, a synapse on a spine can be mimicked by a dendritic synapse of amplitude

$$g'_{syn} = \frac{g_{syn}}{1 + R_n g_{syn}}. \tag{12.15}$$

We see that unless the product of the spine neck resistance with the synaptic conductance change is on the order of unity (or larger), the effect of the spine can be neglected.

The observation that spine necks probably do not contribute toward modulating synaptic weight agrees with experimental evidence regarding the mechanisms underlying the expression of LTP in the hippocampus. While the specific pathways and sites of action remain controversial, there is little to suggest that a postsynaptic change in the electrical impedance of the spine is involved (see the next chapter). This conclusion is also likely to hold in the neocortex, unless synaptic conductance changes are substantially larger and spines thinner and longer than in hippocampus.

12.3.3 Joint Excitatory and Inhibitory Input to a Spine

As mentioned above, it has been a consistent observation that between 5 and 15% of all spines in the cortex carry symmetrical, GABAergic synaptic terminals. Almost always, these same spines are also contacted by excitatory synapses. Such a pair of excitatory and inhibitory synapses localized on a single spine would be the ultimate in highly specific microcircuitry.

Koch and Poggio (1983a,b; see also Diamond, Gray, and Yasargil, 1970) proposed that such a *dual* synaptic arrangement can implement a temporally and spatially very specific veto operation on the basis of the nonlinear interaction between excitation and inhibition of the silent or shunting type (see Sec. 5.1). Indeed, they found that fast $GABA_A$ inhibition can reduce the EPSP in the spine to very small levels provided that it arrived within a very tight time window around the onset of excitation (Fig. 12.7A). According to these numerical solutions to the linear cable equation, such a microcircuit implements an AND-NOT gate with temporal discrimination at the 0.1 msec level.

The degree of temporal specificity, caused by the exceedingly small capacitance in the spine head, can be quantified by the use of the *input delay* in the spine $D_{sp,sp}$ (Secs. 2.4 and 3.6.2). Following Agmon-Snir and Segev (1993), this corresponds to the delay between the centroid of the synaptic current and the centroid of the local EPSP. On the basis of the electrical model of the spine illustrated in Fig. 12.5 and neglecting the tiny current loss across the spine head membrane, we have

$$D_{sp,sp} \approx \frac{\tilde{K}_{dd}}{\tilde{K}_{dd} + R_n} D_{dd} \tag{12.16}$$

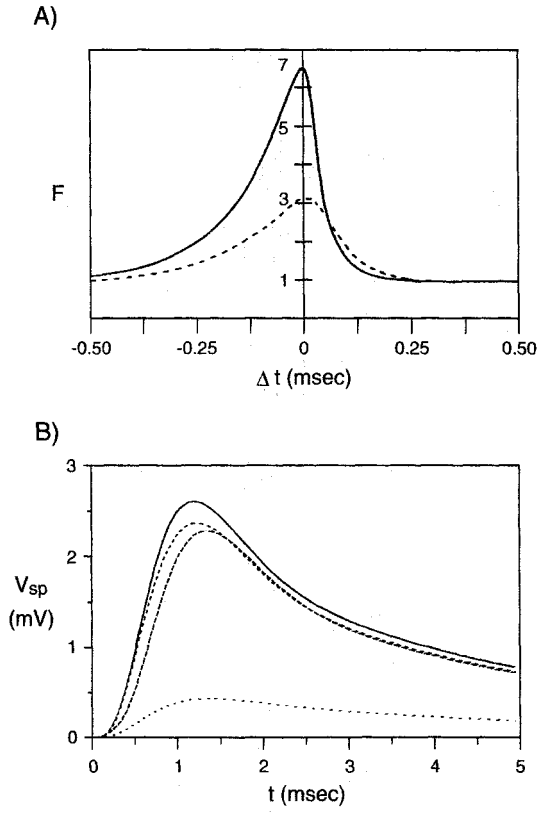

Fig. 12.7 AND-NOT GATING AT THE LEVEL OF A SINGLE SPINE Nonlinear interaction of the AND-NOT type between a fast excitatory synaptic input (of the AMPA type) and inhibition at a single spine. **(A)** The effectiveness of silent $GABA_A$ inhibition in reducing excitation when both are colocalized either on the spine (solid curve) or on the dendrite at the base of the spine (dotted curve). The curve shows the F factor (Eq. 5.14), that is, the ratio of EPSP without inhibition to the mixed excitatory-inhibitory potential, as a function of the onset of inhibition relative to excitation. The half-widths of the curves are 0.12 and 0.22 msec for the spine and dendrite case, respectively. The linear cable equation for a spine located on a pyramidal cell was solved with $t_{peak} = 0.25$ msec for both excitation and inhibition, $E_i = 0$ and $E_e = 80$ mV. Reprinted in modified form by permission from Koch and Poggio (1983b). **(B)** Time course of the spine membrane potential (relative to rest) for the nonlinear Nernst-Planck electrodiffusion model. Here a small EPSP (solid line; $t_{peak} = 1$ msec, $G_{Na} = 0.1$ nS) can be effectively vetoed by a hyperpolarizing potassium conductance increase (due to a $GABA_B$ inhibition with $t_{peak} = 1$ msec, $G_K = 1$ nS; lower dotted curve), while the same or a hundred times stronger conductance change associated with silent inhibition of the $GABA_A$ type (intermediate dashed curves) had almost no effect. Reprinted in modified form by permission from Qian and Sejnowski (1990).

where D_{dd} is the local dendritic delay at the base of the dendrite. If the spine neck is sufficiently thin and elongated, the time window during which inhibition can effectively veto excitation can be a fraction of the corresponding dendritic time window. This effect is particularly strong for spines close to the soma—providing an isolated environment for excitation and inhibition to interact on a very small time scale—while the local spine delay for spines in the distal dendritic tree will be close to the local dendritic delay ($\tilde{K}_{dd}/R_n \to \infty$).

However, as described in Sec. 11.3, for very thin processes it is important to account

for the change in the relevant ionic concentrations. In the case of a spine, even small synaptic inputs can significantly alter the reversal potentials for chloride and potassium, both across the membrane and between the spine head, neck, and the dendrite. This requires solving the nonlinear Nernst-Planck equation as advocated by Qian and Sejnowski (1989, 1990). They studied the interaction between excitation and inhibition on a spine and found that for reasonable inhibitory conductance changes associated with chloride ions (such as would be caused by activation of $GABA_A$ receptors), the intracellular concentration of chloride rapidly increases, bringing the synaptic reversal potential of inhibition substantially above the resting potential, thereby rendering it ineffective (Fig. 12.7B). Indeed, massive activation of $GABA_A$ receptors in thin processes will lead to a depolarization as the chloride concentration gradient decreases, shifting E_{Cl} to progressively more depolarized values. Such "paradoxical" EPSPs have indeed been observed in distal dendrites of pyramidal cells following intense $GABA_A$ activation (Staley, Soldo, and Proctor, 1995).

While shifts in the potassium reversal battery will also occur, rendering $GABA_B$ inhibition equally ineffective for large conductance changes, the situation is quite different for small inputs. Here E_K moves toward the resting potential of the spine, causing a profound reduction in the amplitude of the EPSP without leading to a hyperpolarizing response (Fig. 12.7B). This leads Qian and Sejnowski (1990) to argue that should inhibition play a role in selectively vetoing excitation on a spine or on thin dendrites, that inhibition must be of the $GABA_B$ type (for large dendrites, the advantage reverts to silent $GABA_A$ inhibition). We find no fault in their arguments.

Must dual-input cortical spines necessarily be functional? Dehay et al., (1991) throw the entire idea into doubt by serially reconstructing selected spines that receive geniculate input in cat primary visual cortex. Here, as elsewhere, about 8% of all spines in the input layer (layer 4) carry both an excitatory as well as an inhibitory synaptic input. Because Emerson et al., (1985) as well as Koch and Poggio (1985b) hypothesized that direction and orientation selectivity in visual cortex neurons is mediated by very specific interactions among excitation and shunting inhibition possibly localized on spines, Dehay and colleagues investigated whether geniculo-cortical synapses on spines are a preferred target for inhibition. Using a laborious electron-microscopic reconstruction technique, they showed that these synapses do not have a higher likelihood of being paired with an inhibitory synapse than the majority of synapses originated among cortical cells. Furthermore, in certain cases Dehay et al., (1991) observed an axon from an inhibitory cell making both a synapse on a spine and, a few micrometers away, another synapse on the parent dendrite, revealing a lack of spatial specificity.

At least in cat visual cortex, it appears that dual-input spines could simply be the logical consequence of an imprecise developmental rule that specifies that inhibitory synapses should primarily innervate dendrites and that a small fraction fails to do so.

12.3.4 Geniculate Spine Triad

In other parts of the brain, however, the association between dual synaptic input and spines is much stronger. We encountered already one such *microcircuit* (Rall et al., 1966; Shepherd, 1978) in the mammalian olfactory bulb (Sec. 5.3), which mediates self and lateral inhibition. We will here discuss another instance of a synaptic microcircuit, involving dual input to a spinelike structure.

The mammalian lateral geniculate nucleus (LGN), the midway station for visual input between the retina and the visual cortex, is the site of a very complex synaptic structure known as *glomerulus* (Fig. 12.8). At the heart of each glomerulus lies a terminal from a retinal axon. It is surrounded by the complex intertwining of very thin dendritic processes of a geniculate interneuron with those of a geniculate relay cell (Hamori et al., 1974; Hamos et al., 1985). This circuit is also termed a *triad* because of the intimate association among three different synaptic terminals: the retinal input makes a synapse both on the spine of a geniculate relay cell and on the interneuron. The GABAergic interneuron, in turn, makes a synapse on the geniculate spine.

Retinal output is organized in multiple parallel channels of information. One of these, the X cells, which are particularly sensitive to high spatial frequencies, tends to make the majority of synaptic contacts onto geniculate relay cells and interneurons in association with these spine triads (Wilson, Friedlander, and Sherman, 1984). At least in cat, the Y cells, the other major retinal output pathway, tend to make their synapses directly onto the dendrites of their geniculate target relay cells, bypassing the inhibitory interneurons (Sherman and Guillery, 1996).

Passive cable modeling of geniculate relay cells with the spine-triad local circuit using excitation and shunting inhibition (Koch, 1985) shows that if the size of the inhibitory

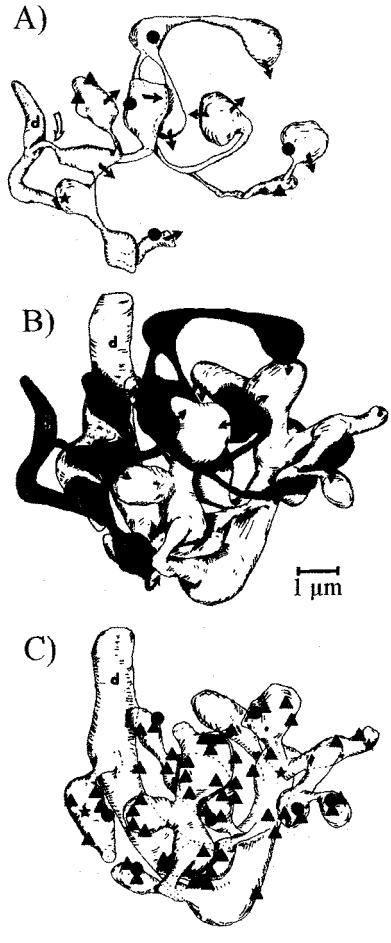

Fig. 12.8 SYNAPTIC SPINE TRIADS IN THE LGN These drawings, based on laborious electron-microscopic reconstructions of cells in the cat LGN (Hamos et al., 1985), illustrate the very intricate and baroque synaptic microcircuits that can be found in the nervous system. The arrangement shown, known as a *glomerulus*, includes **(A)** a dendrite (marked d) of a local inhibitory interneuron from which a dozen very thin processes spring forth. The full circles indicate the location of excitatory synapses from a retinal axon. The interneuron in turn inhibits the geniculate relay cell at the nine sites indicated with full arrows. **(B)** This interneuron (in black) is shown grappling with five spinelike appendages on a dendrite of a geniculate relay cell (in white), which are shown more fully in **(C)**. The full circles indicate nine retinal synapses, and the filled triangles 40 inhibitory synapses from other interneurons. The *triad* is a synaptic arrangement in which an excitatory input (here, an optic nerve axon) excites both an interneuron as well as the geniculate relay cell. The interneuron, in turn, directly inhibits this site. Reprinted by permission from Hamos et al., (1985).

conductance change due to the $GABA_A$ receptors is neither too small nor too large, it can effectively and specifically veto the retinally induced EPSP without inhibiting EPSPs from neighboring synapses. Thus, although the inhibition is postsynaptic, from a functional point of view it acts similar to *presynaptic inhibition*.

Because of the expected 1 or 2 msec delay between retinal input triggering an EPSP in the interneuron and the opening of postsynaptic $GABA_A$ receptors on the spine in response to this input, inhibition is likely to be not very effective at low firing rates (caused, for instance, by a low contrast stimulus). Inhibition would be strongly activated for sustained, high-contrast input. Because the spine-triad circuit is essentially limited to X cells, Y cells should not show any comparable localized and specific type of inhibition. Experimentally, it is known that geniculate cells are more phasic than their retinal counterparts (Cleland, Dubin, and Levick, 1971) and that inhibition is independent of stimulus contrasts for Y cells but increases with increasing stimulus contrast in X cells (Berardi and Morrone, 1984). Finally, it is clear that the level of activity in the interneuron itself will be crucial in determining whether or not it can inhibit the retinal input (Bloomfield and Sherman, 1989). Such context-dependent inhibition could be important, for instance, during saccadic suppression.

We conclude that the spine-triad microcircuit on geniculate X cells appears to implement a specific type of activity-dependent inhibition (Hamori et al., 1974; Koch, 1985).

12.4 Active Electrical Properties of Single Spines

In the mid-1980s, several independent groups worked on the idea of synaptic amplification in dendritic spines endowed with *active, regenerative* electrical properties (Perkel and Perkel, 1985; Miller, Rall and Rinzel, 1985; Shepherd et al., 1985; Pongracz, 1985; Segev and Rall, 1988). At first viewed with skepticism by experimentalists, recent calcium-imaging experiments have shown that spines on hippocampal pyramidal as well as cerebellar Purkinje cells can show all-or-nothing responses (Yuste and Denk, 1995; Denk, Sugimore and Llinás, 1995; see Sec. 12.6.2). It remains to be seen whether these spikes are actually restricted to the spines or whether they invade the neighboring dendrites.

The basic idea is simple and will be explained with reference to the painstakingly executed Segev and Rall (1988; see also Rall and Segev, 1987) study. They endowed the head of a single spine—on an otherwise passive dendrite—with the fast sodium and delayed-rectifier potassium conductances found in the squid axon (adjusted for 20° C and with a tenfold increase in peak conductances; see Fig. 12.9). With a single-channel conductance of about 15 pS (Table 8.1) this corresponds to 1050 sodium channels per spine. Using a very fast synaptic input ($t_{peak} = 0.035$ msec), Segev and Rall found that the amplitude of the synaptic input g_{peak} had to exceed a very sharp threshold in order to generate an all-or-nothing action potential in the spine (Fig. 12.10). Such a tongue-twisting "spine spike" will be initiated once V_{sp} exceeds a critical voltage threshold V_{th} (see the discussion in Secs. 6.3.1 and 19.2). At V_{th}, the sum of the synaptic and active spine currents exceeds the current I_n flowing through the spine neck and onward into the dendrite.

In the suprathreshold domain, the amplification that can be obtained with a small number of strategically placed active channels on a spine is evident in the lower graph of Fig. 12.10. The 90 mV spine action potential is attenuated across the 1000 MΩ neck but still leads to a 5 mV EPSP at the base of the spine. Contrariwise, a passive spine would have depolarized to 27 mV, of which only about 1 mV would have survived the attenuation through the spine neck (dotted lines in Fig. 12.10). Thus, a tiny 1 μm^2 patch of active channels leads to a fivefold voltage amplification.

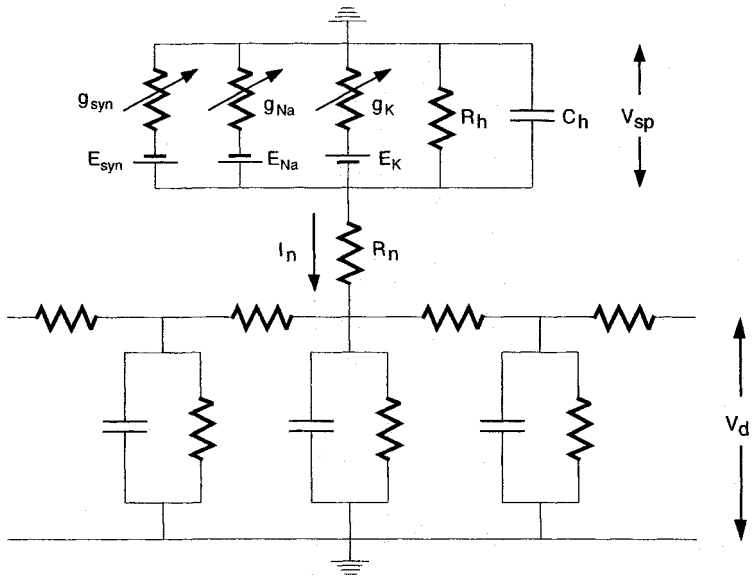

Fig. 12.9 MODEL OF AN ACTIVE SPINE Lumped electrical model of an active spine, as used in the Segev and Rall (1988) study. The spine head is endowed with squid axon membrane (at 20° C, but with a tenfold increase in the maximal conductances $\overline{G}_{Na}$ and $\overline{G}_K$). With $C_m = 1\ \mu F/cm^2$, the passive time constant in the spine at rest is 1.4 msec. The synaptic input is very fast, with $t_{peak} = 0.035$ msec and $E_{syn} = 100$ mV. A tenfold slower synaptic input is expected to yield a similar behavior in the presence of a tenfold slower membrane time constant. The input resistance at the base spine is 262 MΩ.

The amplitude (as well as the integrated area) of the dendritic EPSP is independent of variations in g_{peak} (as long as g_{peak} is above threshold; Fig. 12.10), since the maximal value of V_{sp} is determined by the height of the action potential, which is rather fixed. Given the large variability in the postsynaptic amplitude of individual synaptic inputs at cortical synapses (see, Fig. 4.4), active spines can thereby eliminate a source of uncertainty associated with passive spines (as well as amplify their responses).

Figure 12.11 illustrates the dependency of V_{sp} and V_d on the spine neck resistance. For small values of R_n (here below 620 MΩ), the spine input impedance $\tilde{K}_{sp,sp}$ is not sufficiently high in order for the local EPSP to exceed V_{th}: the peak value of both V_{sp} and V_d in the presence of sodium and potassium channels is little different from the peak value of the potential in the passive situation (right panels in Fig. 12.11). For $R_n = 630$ MΩ, a spike is generated after a short delay, while for the high resistance neck (curve b), an action potential is established in a very secure manner and with a larger amplitude. Seemingly paradoxically, however, the amplitudes of the resulting EPSPs at the dendrite are reversed. While a larger spine neck resistance increases the spine input impedance (witness Eq. 12.4), thereby facilitating spike generation, it also causes a larger voltage attenuation across the spine neck. In the limit of an infinitely thin spine neck, the smallest input will cause V_d to "lock up" at E_{syn}; yet none of that will be visible at the base of the spine. (For all the subtleties of this dependency, see Segev and Rall, 1988.) As the lower right panel in Fig. 12.11 best summarizes, amplification over the passive spine is obtained within a narrow range of R_n. Given the inverse quadratic dependency of R_n on d_n (Eq. 12.1), this translates into a very strong dependency of V_d on the spine neck geometry.

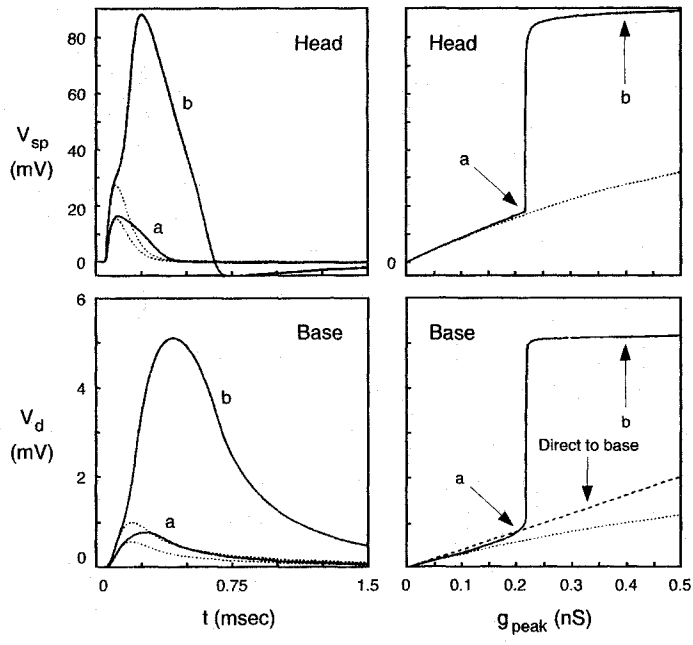

Fig. 12.10 Active Spines as a Function of the Input Amplitude Time course and peak depolarization in the spine and dendrite shown in Fig. 12.9 as a function of the amplitude of the fast (t_{peak} = 0.035 msec) voltage-independent synaptic conductance change g_{peak}. The two left panels illustrate $V_{sp}(t)$ and $V_d(t)$ for two values of g_{peak} (0.2 nS for *a* and 0.4 nS for *b*) while the right panels plot the peak values of V_{sp} and V_d as a function of the input amplitude. R_n is always set to 1 GΩ. Dotted curves are for a passive spine, whereas the solid curves are for an active spine. Close inspection of these plots reveals some minimal evidence of active channels for the smaller inputs of the two. If the input is doubled, a very robust all-or-none spike is initiated. Further increases of g_{peak} have no further effect on the peak of either V_{sp} or V_d. The dashed line in the lower right panel shows the peak of V_d when the same synaptic input is applied directly to the passive dendrite, rather than to the spine. Active spines can be used to amplify synaptic input. Reprinted by permission from Segev and Rall (1988).

At present, we do not know whether sodium channels are present on dendritic spines. However, phenomena similar to those discussed here could be instantiated with slower calcium-mediated all-or-none spine spikes. Two-photon microscopy experiments using calcium dyes have provided tantalizing preliminary evidence for all-or-none calcium events following synaptic input onto spines of hippocampal and Purkinje cells (see Sec. 12.6.2).

What Segev and Rall (1988; see also Perkel and Perkel, 1985; Miller, Rall, and Rinzel, 1985; Shepherd et al., 1985) demonstrate is that active spines can significantly amplify (two to tenfold) synaptic input at minimal metabolic costs (only requiring the insertion of voltage-dependent channels into a very small membrane patch the size of a spine head). We conclude that active spines could provide the biophysical substrate for *information storage* as well as *information processing*.

The strong dependency of V_d on parameters associated with spine neck geometry provides the cell with a sensitive mechanism to modulate the synaptic weight of individual inputs. Only within a narrow range of R_n will the synaptic input be high; outside of this range, the dendritic EPSP will be much reduced. At the same time, this sensitivity also represents the Achilles heel of the hypothesis: as evidenced by the large degree of variability in the

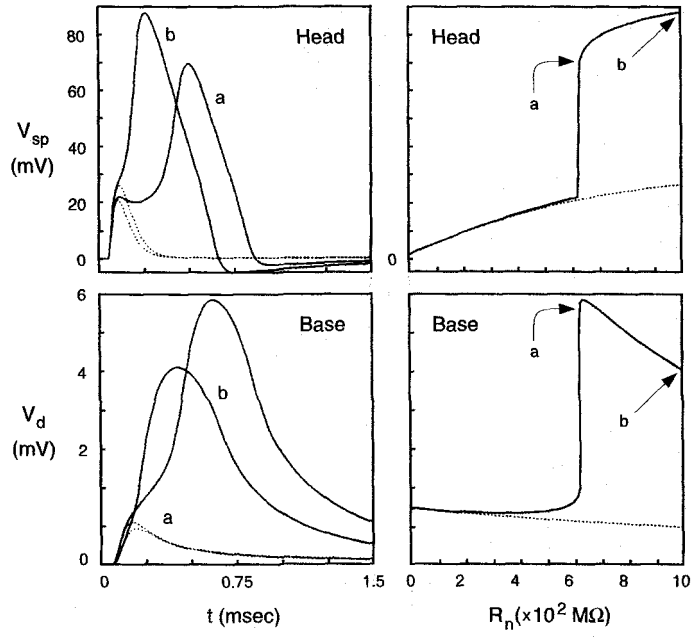

Fig. 12.11 Active Spines as a Function of the Spine Neck Resistance Time course and peak depolarization in the spine and dendrite shown in Fig. 12.9 as a function of the spine neck resistance (for $g_{peak} = 0.37$ nS and $t_{peak} = 0.035$ msec). The two left panels illustrate $V_{sp}(t)$ and $V_d(t)$ for $R_n = 630$ MΩ (curve *a*) and $R_n = 1000$ MΩ (curve *b*) while the right panels plot the peak values of V_{sp} and V_d as a function of R_n. Dotted curves are for a passive spine, whereas the solid curves are for an active spine. Large amplification of the dendritic EPSP with respect to a passive spine only occurs in a relatively narrow range of R_n values: if the neck is too short or too thick, the electrical decoupling of excitable channels at the spine head from the rest of the cell is insufficient to initiate an action potential, while for very thin and long spine necks (implying large values of R_n), the attenuation across the spine neck is excessive. This dependency on spine neck geometry could be exploited in synaptic plasticity. Reprinted by permission from Segev and Rall (1988).

spine neck geometry (Fig. 12.4), the brain might not be able to control spine neck geometry with sufficient accuracy to exploit it in a consistent manner.

What remains unclear from an experimental point of view is whether action potentials are restricted to the spines themselves or whether they spread to the parent dendrite. As witnessed by Fig. 12.11, a true spiking spine requires a very thin or elongated neck to achieve the necessary isolation from the parent dendrite.

More interesting from the point of view of neuronal computation are the combinatorial possibilities for nonlinear interactions among active spines on distal dendrites. Under certain circumstances, one or a small number of simultaneous inputs to active spines can trigger action potentials in neighboring spines. We will pick up the threads of this story in Sec. 19.3.2.

12.5 Effect of Spines on Cables

Given the large spine density (up to 10 spines per micrometer of dendrites), 50% or more of the total neuronal membrane area resides in spines. It is therefore important to account for

this additional area to properly analyze the propagation of electrical signals in the dendritic tree. Although these effects provide no insight into the function of spines, they may be ironically the only ones that we can infer with confidence to be important.

Accounting for the effect that spines have on cable propagation is based on the assumption that for current flow from the dendrite back into the spine the membrane area of the spine can be incorporated into the membrane of the parent dendrite. As we expect from basic cable theory and as discussed more fully below, there exists almost no voltage attenuation from the dendrite back into the spine (contrary to the voltage attenuation from the spine into the dendrite). This isopotentiality is the reason that the spine area can be lumped into the overall area of the dendrite. Several different methods to deal with this problem have been proposed, based on the intuition that in the presence of a large number of spines, the total capacitance will increase while the membrane resistance will decrease.

One method (Stratford et al., 1989) transforms the spiny dendrite (with diameter d and length l) into a single "equivalent" (and smooth) cylinder, whose diameter d' and length l' are larger than those of the parent dendrite by some fraction $\mathcal{F}$, with

$$\mathcal{F} = \frac{A_{\text{dend}} + A_{\text{spine}}}{A_{\text{dend}}} \tag{12.17}$$

where A_{dend} is the total membrane area of the "stem" dendrite without any spines, and A_{spine} is the total membrane area of all spines (spine necks and spine heads) on the dendrite. The dimensions of this equivalent cable are

$$l' = l\mathcal{F}^{2/3} \tag{12.18}$$

and

$$d' = d\mathcal{F}^{1/3}. \tag{12.19}$$

Solving for the membrane potential in a cable studded by n spines requires the solution of $2n + 1$ coupled equations (assuming that each spine is modeled using two compartments, one for the neck and one for the head). The transformation described here reduces this to solving the cable equation in a single, unbranched cylinder. The effective area of the cable is scaled by $\mathcal{F}$, its infinite input resistance by $\mathcal{F}^{-1/2}$, and its electrotonic length of the equivalent cable by $\mathcal{F}^{1/2}$. The time constant remains unchanged. The transformed segment behaves like the spiny original under most circumstances (Stratford et al., 1989).

An alternative transformation method (Shelton, 1985; Holmes, 1989; Segev et al., 1992) preserves the dimensions of the dendrite but scales C_m and R_m appropriately by

$$R'_m = \frac{R_m}{\mathcal{F}} \tag{12.20}$$

and

$$C'_m = C_m\mathcal{F}. \tag{12.21}$$

Both methods are mathematically equivalent.

A novel analytical method to incorporate spines into the continuous cable equation was developed by Baer and Rinzel (1991). It is powerful, since it can deal with passive as well as active spines. Baer and Rinzel replace the cable equation for a single passive cable by two equations, one for the voltage along the dendrite $V_d(x, t)$ and one for the voltage in the spines $V_{sp}(x, t)$. The density of spines per unit electrotonic length of cable is $s(x)$. A single spine receives synaptic input current $I_{\text{syn}}(x, t)$ (which can vary with the position of

the spine along the cable), generating a local current across the spine head I_{ionic} that can include Hodgkin–Huxley or other voltage-dependent currents. Spines are independent of each other, only interacting with the dendrites via the neck current I_n that flows through the spine neck. The associated cable equation can be expressed as

$$\tau \frac{\partial V_d}{\partial t} = \lambda^2 \frac{\partial^2 V_d}{\partial x^2} - V_d + s(x) R_\infty I_n \tag{12.22}$$

$$C_h \frac{\partial V_{sp}}{\partial t} = -I_{\text{ionic}} - I_n - I_{\text{syn}}(x, t) \tag{12.23}$$

with an additional equation for the neck current,

$$I_n = \frac{V_{sp} - V_d}{R_n}. \tag{12.24}$$

Here τ, λ and R_∞ are the time and space constants and the input resistance of a semi-infinite cable in the absence of any spines, and C_h is the tiny spine head capacitance (Fig. 12.5).

Baer and Rinzel (1991) go on to solve these equations for active as well as passive spines. In the former case, wavelike propagation can occur along the passive cable, supported by the amplifying spines. In the latter case, both equations are linear and $I_{\text{ionic}} = V_{sp}/R_h$. Assuming a constant density of spines, $s(x) = s$, and steady-state conditions, they compute the effective electrotonic length of a spiny dendrite as

$$L' = L\sqrt{1 + sR_\infty/(R_n + R_h)} \tag{12.25}$$

and the infinite input resistance as

$$R'_\infty = \frac{R_\infty}{\sqrt{1 + sR_\infty/(R_n + R_h)}}. \tag{12.26}$$

Since under almost all circumstances $R_h \gg R_n$, these reduce to

$$L' = L\mathcal{F}_{1/2} \tag{12.27}$$

and

$$R'_\infty = R_\infty \mathcal{F}^{-1/2} \tag{12.28}$$

as in the more heuristic methods discussed at the beginning of this section.

In summary, all of the spine-replacement methods discussed here conclude that the collective effect of dendritic spines is to increase the effective membrane capacitance and decrease the membrane resistance, leading to a lower input resistance and an increased electrotonic length compared to a smooth dendrite of equal diameter and physical length (Wilson, 1988). Indeed, Jaslove (1992) argues that these population effects—influencing the degree of spatio-temporal integration occurring in the dendrites—are the primary functional reason for why some cells are studded with spines while others are devoid of them.

12.6 Diffusion in Dendritic Spines

So far, we have focused exclusively on the electrical properties of spines. Yet, over the last decade, an alternative view of spines has emerged which emphasizes their effect on chemical, rather than electrical, signaling. As discussed in Chap. 13, chemical dynamics of

intracellular calcium and other second messengers in the spine are of particular importance in the induction of long-term potentiation.

12.6.1 Solutions of the Reaction-Diffusion Equation for Spines

Compartmental modeling of calcium diffusion and binding following synaptic input to the spine (Robinson and Koch, 1984; Coss and Perkel, 1985; Gamble and Koch, 1987; Wickens, 1988) played a trail-blazing role here, followed a few years later by the experimental study of calcium dynamics in single spines (Müller and Connor, 1991; Guthrie, Segal and Kater, 1991; Jaffe, Fisher, and Brown, 1994; Eilers, Augustine, and Konnerth, 1995; Yuste and Denk, 1995; Denk, Sugimore, and Llinas, 1995; Svoboda, Tank, and Denk, 1996). More recent modeling studies have, of course, become much more sophisticated and use a very fine grained spatial resolution to keep track of substances in the spine head and neck (Holmes and Levy, 1990; Zador, Koch, and Brown, 1990; Koch, Zador, and Brown, 1992; DeSchutter and Bower, 1993; Gold and Bear, 1994; Zador and Koch, 1994; Woolf and Greer, 1994; Jaffe, Fisher and Brown, 1994).

The principal ideas are really very simple, in particular in light of the linearized reaction-diffusion equation discussed in Sec. 11.7. Using the geometry of Fig. 12.12A, and in the presence of low calcium concentration, a linear nonsaturable calcium pump in the spine neck and head membrane, and a fast second-order nondiffusible buffer, the reaction-diffusion equations (Eqs. 11.48) in the presence of calcium pumps can be reduced to the linear partial differential equation (Eq. 11.51), formally identical to the cable equation.

This allows us to define the "chemical input resistance" (Carnevale and Rosenthal, 1992; Zador and Koch, 1994), in analogy to the standard electrical input resistance, as the change in calcium concentration in response to a current of calcium ions (Table 11.2). Both the chemical and the electrical spine input resistances are much larger than the associated dendritic input resistances. At the spine head, the input resistance is 4.2×10^{-2} μM/fA while the dendritic input resistance is 4.8×10^{-3} μM/fA. In other words, a sustained calcium current injected into the spine head leads to a tenfold larger increase in calcium concentration than the same current applied at the dendritic shaft.

A key difference between the electrical and the chemical properties of spines arises from the effect of the spine neck. In our analysis, as well as in almost all published studies of the electrical properties of spines, the electrical cable properties associated with the spine neck are neglected, since no significant current will cross the membrane of the 1-μm long "cable," a direct consequence of the large value of λ. In order to estimate the loss of calcium current through the spine neck membrane, we compute the space constant of Eq. 11.55 associated with the linearized reaction-diffusion equation. Reading off from Fig. 11.9, λ_{r-d} for a 0.1 μm thin cable is 0.46 μm (0.27 μm without diffusible buffer). Because the dendritic shaft is more than $2\lambda_{r-d}$ away from the spine head, the calcium concentration at the shaft is expected to be tenfold lower than at the head. This is in dramatic contrast to the almost complete lack of electrical current attenuation experienced between the spine head and the base (λ is close to three orders of magnitude larger than λ_{r-d}; Fig. 11.9).

These principles are illustrated in simulations of the fully nonlinear calcium dynamics thought to underly the induction of LTP (Zador, Koch, and Brown, 1990; Brown et al., 1991b). In the model, synaptic input activates a fast non-NMDA conductance (Eq. 4.5) as well as an NMDA voltage-gated conductance (Eq. 4.6; Fig. 12.12A). 2% of the NMDA current is assumed to be carried by Ca^{2+} ions. Subsequent to entry into the intracellular cytoplasm, these ions can bind to one of the four calmodulin binding sites (Fig. 11.7),

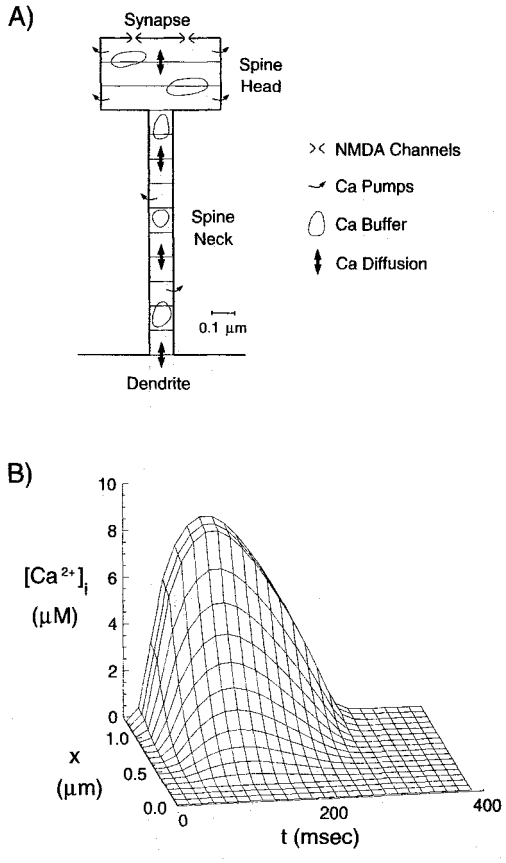

Fig. 12.12 SPATIO-TEMPORAL DYNAMICS OF CALCIUM IN A SPINE **(A)** Compartmental representation for solving the reaction-diffusion equation associated with the system controlling intracellular calcium in response to a mixed excitatory voltage-independent non-NMDA and a voltage-dependent NMDA synaptic input. Opening of the NMDA channels causes an influx of calcium ions. These are removed by the action of membrane-bound pumps in the spine head and neck, by binding to cytoplasmic calcium buffers, as well as by diffusion into the dendrite. The drawing is to scale, with $d_n = 0.1$ μm. The individual compartments are shown by thin lines. **(B)** Spatio-temporal dynamics of Ca^{2+} in response to a train of three presynaptic stimuli (at 100 Hz) while the membrane potential in the spine was simultaneously clamped to -40 mV (mimicking a somatic voltage-clamp protocol). Changes in $[Ca^{2+}]_i$—induced by the calcium influx through the NMDA channel—are restricted mainly to the spine head. x indicates the distance from the dendritic shaft (with 0 corresponding to the shaft and $x = 1.3$ μm to the subsynaptic cleft). Reprinted by permission from Zador, Koch, and Brown (1990).

they can be pumped out of the cell via two different pumps, and they can diffuse along the spine neck and out into the dendrite (assumed to be an infinite capacity sink with a resting calcium level of 50 nM). Simulated calcium dynamics following a train of synaptic stimuli are shown in Fig. 12.12B. Due to the tiny volume of the spine, the small Ca^{2+} influx following synaptic stimulation leads to a large transient increase in the spine calcium concentration (here, $[Ca^{2+}]_{sp} = 10\,\mu M$ corresponds to about 350 Ca^{2+} ions). We conclude that spines can amplify the small incoming calcium signal dramatically. Yet due to the large mismatch in volumes and the associated small chemical input impedance at the dendrite, the

large peak changes in $[Ca^{2+}]_i$ at the spine cause the dendritic level of $[Ca^{2+}]_i$ to fluctuate only by several tens of nanomolars.

Due to the difference in input impedances between the spine and the dendrite, both calcium and voltage will be severely attenuated when going from the spine to the dendrite, even though no current is lost across the spine neck membrane in the case of the cable equation. This is illustrated in a different manner in Fig. 12.13, showing both voltage and calcium attenuation along the spine, that is, the ratio of the voltage (or calcium concentration) at one location to the voltage (or calcium concentration) at another location.

Quite a dramatic difference emerges when considering antidromic attenuation. When voltage clamping the dendrite to any particular value, the voltage at the spine head will be attenuated by the factor (Eq. 3.34)

$$A_{d,sp} = \frac{\tilde{K}_{dd}}{\tilde{K}_{sp,d}}. \tag{12.29}$$

Since $\tilde{K}_{sp,d} \approx \tilde{K}_{dd}$ (Eq. 12.5) to a pretty good approximation, no voltage attenuation is expected into the spine, as confirmed by the upper dashed line in Fig. 12.13. However, due to the sustained loss of calcium ions as they are being pumped through the spine neck membrane into the extracellular cytoplasm, the effective value of $\tilde{K}_{sp,d}$ for the reaction-

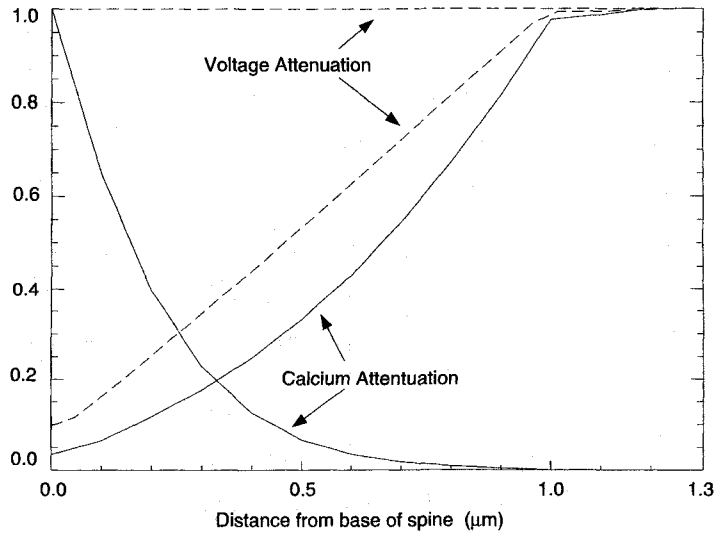

Fig. 12.13 Voltage and Calcium Attenuation in and out of a Spine Voltage and calcium attenuation for two different simulations as a function of the distance from the dendrite (at 0; the spine neck ends at 1 μm and the spine head extends from 1 to 1.3 μm). The upward diagonal dashed and solid curves illustrate voltage and calcium attenuation from the spine into the dendrite. These curves are taken from the simulation shown in Fig. 12.12B and indicate peak calcium and voltages following three presynaptic stimuli to the spine synapse. Both variables attenuate about tenfold. In a different simulation illustrating antidromic *steady-state* behavior, either the calcium (downward going solid curve) or the voltage (constant dashed line) is clamped to a fixed value in the dendrite. Due to the presence of calcium pumps in the spine neck, calcium rapidly attenuates and reaches baseline levels at the spine head. The membrane potential, however, does not attenuate across the spine neck due to the negligible current loss across the spine neck and head membranes. Reprinted by permission from Koch and Zador (1993).

diffusion system is very low. As a consequence, when the calcium concentration in the dendrite is "clamped" to 1 μM, the calcium attenuation into the spine head is very large: it remains protected from the high dendritic calcium values by the presence of calcium pumps in the membrane of the spine neck (Zador, Koch, and Brown, 1990; Koch, Zador, and Brown, 1992), providing a graphic illustration of the tiny size of the associated space constant. Given the square-root dependency of λ_{r-d} on the density of pump molecules in the membrane (Table 11.3), this density would have to change substantially before any significant effect of dendrite calcium on the spine head would be seen. Or, short and sweet, "spines are electrically coupled but chemically isolated from changes occurring in the dendrite." Of course, the presence of the spine apparatus or other organelles would further impede the flow of calcium ions into the spine head. What applies to calcium will, of course, also apply to other second messenger systems (see also Woolf and Greer, 1994).

The value of many of the relevant biophysical and biochemical parameters can only be specified within a factor of 2, 5, or even 10. For instance, relatively small changes in the spine neck geometry or in the buffer concentration can cause the peak calcium concentration in the spine head to vary quite a bit. Whether this sensitivity of peak $[Ca^{2+}]_{sp}$ subserves a function, as contended by Gold and Bear (1994) (Fig. 13.7) is not known.

One obvious effect that should be emphasized is that the electrical as well as the chemical input impedance increases with increasingly longer and thinner spines. If the establishment of LTP were to depend on exceeding either a voltage threshold or a critical concentration of $[Ca^{2+}]_i$, the thin and elongated spines would be in a better position than the short, stubby ones to achieve this. Conversely, since the synaptic weight depends little on the spine neck—for the range of geometries reported in hippocampus and for passive spines—stubby spines could be considered to be permanently modified, while elongated or thin spines would constitute a reservoir that can be recruited for long-term synaptic potentiation as well as for long-term depression. Indeed, several reports have emphasized that high-frequency synaptic stimulation that causes LTP leads to an excess of short or thick spines (Lee et al., 1980; Chang and Greenough, 1984).

Although we mainly use arguments from linear cable theory, the simulations in Figs. 12.12 and 12.13, based as they are on the peak transient calcium concentration changes in the full nonlinear model, confirm these expectations.

12.6.2 Imaging Calcium Dynamics in Single Dendritic Spines

While it remains technically impossible to record spine EPSPs directly, a number of groups are "pushing the technological envelope" by imaging calcium activity in dendrites and in individual spines via calcium-sensitive fluorescent dyes (Müller and Connor, 1991; Guthrie, Segal, and Kater, 1991; Regehr and Tank, 1992; Jaffe, Fisher, and Brown, 1994; Yuste and Denk, 1995; Segal, 1995a; Eilers, Augustine, and Konnerth, 1995; Denk, Sugimore, and Llinás, 1995; for a review see Denk et al., 1996). The more recent studies make use of confocal laser scanning or two-photon fluorescence microscopy. They confirm that in the absence of calcium entry through voltage-dependent calcium channels, spines do isolate in both directions: a high calcium concentration in the dendrite is frequently not paralleled by an equally high concentration change in the spine (Fig. 12.14C). Control experiments with injected cobalt indicate that the lag is not due to a physical diffusion barrier between the dendrite and the spine (Guthrie, Segal, and Kater, 1991), supporting the idea that calcium-dependent processes, such as calcium pumps or other uptake systems, were responsible for isolating the spine head. Conversely, synaptic stimulation leads to restricted calcium

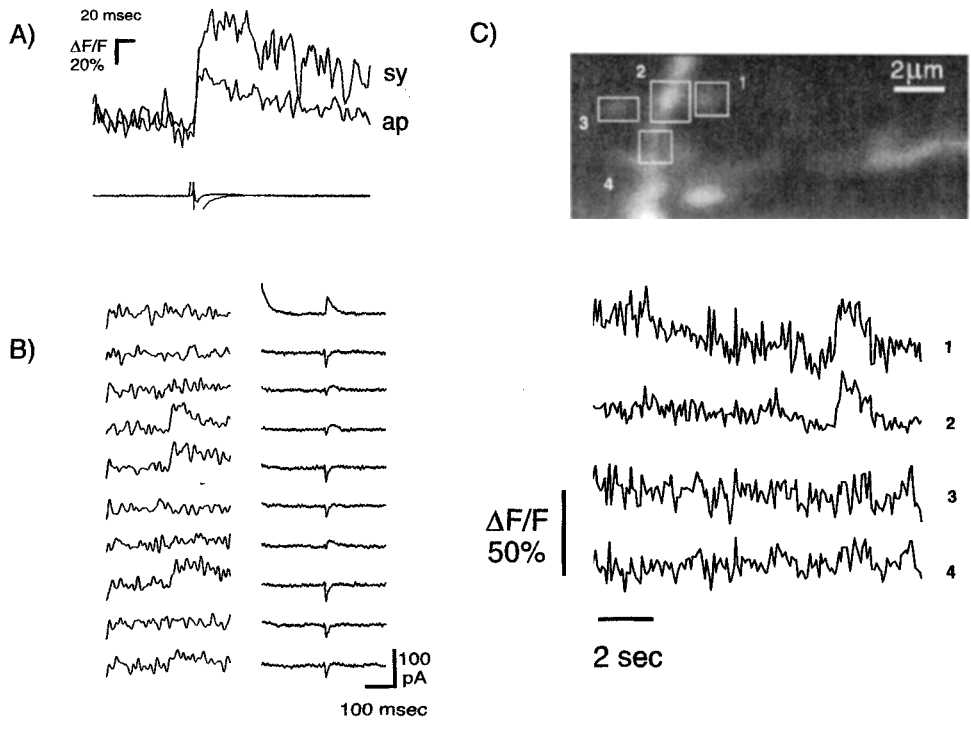

Fig. 12.14 Imaging Calcium in a Single Spine Fluorescence signal from a single spine on a CA1 pyramidal cell in a rat hippocampus slice. **(A)** Using two-photon microscopy, Yuste and Denk (1995) record the increase in fluorescence of a calcium indicator, due to an increase in free intracellular calcium, evoked either by spontaneous synaptic activity (sy) or by the antidromic invasion of a postsynaptic action potential (ap). Following synaptic input, calcium rises within 2 msec, the temporal resolution of the measurement. The influx of calcium in response to a postsynaptic spike is mediated by voltage-dependent calcium currents in the dendrites and spines. **(B)** Stochastic failure of synaptic transmission at the same spine can also be visualized. Left column: fluorescence measurements in response to subthreshold synaptic stimulation. Right column: simultaneous current recording at the soma. In only three cases is a clear synaptic response evident at the single spine. Only in about 20 to 40% of the cases will a presynaptic spike cause release of a synaptic vesicle and a postsynaptic response. **(C)** Spontaneous synaptic activity causes an increase in $[Ca^{2+}]_i$ at a single spine (1) and the adjacent dendritic shaft (2), while a neighboring spine (3) or dendrite (4) shows no such increase. Later during the same recording session, a synaptic-evoked calcium accumulation was restricted to the spine (3). Reprinted by permission from Yuste and Denk (1995).

increase in individual spines but not in the dendrite, confirming the basic aspects of the models discussed above. Indeed, the resolution of these methods is such that stochastic failure of synaptic transmission can be observed in the calcium response at a single spine (Fig. 12.14B).

In real life, things become more interesting, but also more complicated, by the presence of high-threshold noninactivating voltage-dependent calcium channels in dendrites and spines: both somatic depolarization via an intracellular electrode and antidromic spike invasion lead to calcium increases in dendrites and in spines throughout the cell (Fig. 12.14A; Markram, Helm, and Sakmann, 1995; Sec. 19.1). With the exception of Robinson and Koch (1984) and Gamble and Koch (1987), previous compartmental models have assumed that all calcium entry occurs via the activated NMDA synaptic receptors at the stimulated

spine. Since antidromic spike invasion does occur under physiological conditions and may indeed be facilitated by the presence of sodium channels on the apical dendrites (Stuart and Sakmann, 1994; Secs. 19.1 and 19.2.2), it is unclear what this implies about the specificity of LTP, which is generally believed to be restricted to the stimulated synapse (see the following chapter). It might well be that under physiological conditions the critical calcium concentration required to initiate the biochemical cascade that leads to the enhancement of the synapse cannot be achieved unless calcium accumulation from synaptic (calcium entry via NMDA and non-NMDA receptors; Schneggenburger et al., 1993) as well as nonsynaptic (voltage-dependent calcium channels and calcium-triggered calcium release; Regehr and Tank, 1992) sources cooperate.

12.7 Recapitulation

The small extent of dendritic spines, somewhat smaller than the average-sized *Escherichia coli* colon bacterium, precluded until very recently direct experimental access, making the function and properties of dendritic spines a favorite subject among modelers. Hypotheses concerning their function can be divided into two major categories: spines as devices for the induction and/or the expression of synaptic plasticity and spines as devices subserving specific computations. Other proposals have been advanced, such as that spines primarily serve to connect axons with dendrites (Swindale, 1981), that spines serve to increase the effective membrane capacity of a dendrite (Jaslove, 1992), or that spines serve to protect the dendrite from high, and therefore possibly toxic, overdoses of calcium during synaptic activation (Segal, 1995b). While each of these ideas may contain some grain of truth, we here emphasize those properties of spines of direct relevance to information processing and storage.

That changes in the electrical resistance of the spine neck can modulate the EPSP amplitude of a synapse on this spine has been a popular idea since it was discussed in detail by Rall (1970, 1974). It now appears, at least in the case of hippocampal CA1 pyramidal cells (but most likely also for neocortical spines), that the spine neck conductance is too large relative to the synaptic-induced conductance change to be able to effectively modulate the dendritic EPSP for *passive* spines. Furthermore, as covered in the following chapter, the weight of the evidence leans in favor of a pre- rather than a postsynaptic site as the locus where the long-term changes in synaptic weight are affected. It is most likely in the induction phase of Hebbian long-term changes in synaptic plasticity that spines play a critical role.

Both theoretical and experimental evidence is accumulating that spines may create an isolated biochemical microenvironment for inducing changes in synaptic strength. In the induction of associative (or Hebbian) LTP, for example, the spine could restrict changes in postsynaptic calcium concentration to precisely those synapses that met the criteria for potentiation. Furthermore, changes in spine shape could control the peak calcium concentration induced by synaptic input: all other factors being equal, long and skinny spines would have higher peak calcium levels than short and stubby spines. This could provide an alternative explanation for some of the environmental effects on spine morphology. The biochemical compartmentalization provided by dendritic spines could, of course, be equally crucial for a number of other diffusible second messengers, such as IP_3, calmodulin, cyclic AMP, and others. We conclude that while spines may not play any role in the expression of synaptic plasticity, they may be crucial in the induction phase by offering a protected microenvironment for calcium and other messenger molecules.

Spines can provide a very rich substrate for computation if they are endowed with regenerative, all-or-none electrical properties as experimental data are now suggesting. The elevated spine input resistance, as compared to the input resistance of the parent dendrite, and the partial electrical isolation of the spine from the rest of the cell, could make spines a favorable site for the initiation of action potentials. The proposal that spines contain voltage-dependent membrane conductances, first advanced by theoreticians and now experimentally supported by evidence for calcium spikes, implies that a dendritic spine is a basic computational gate with two states, on or off. Modeling studies, treated in Sec. 19.3.2, demonstrate that a population of strategically placed active spines can instantiate various classes of quasi-Boolean logic. The combination of excitatory and inhibitory synapses on a single spine—whether passive or active—observed in certain brain areas can only enhance this computational power. With up to 200,000 spines on certain cell types, it remains to be seen whether the nervous system makes use of this vast computational capacity.